Int. J. Heat Mass Transfer. Vol. 31, No. 2, pp. 419–427, 1988
Printed in Great Britain

0017–9310/88 $3.00 + 0.00

Boundary and inertia effects on conjugate mixed convection heat transfer from a vertical plate fin in a high-porosity porous medium

U. S. GILL† and W. J. MINKOWYCZ
Department of Mechanical Engineering, University of Illinois at Chicago, Box 4348, Chicago, IL 60680, U.S.A.

(*Received* 1 *September* 1987)

Abstract—Conjugate mixed convection heat transfer along a vertical plate fin embedded in a saturated high-porosity porous medium has been studied. A local non-similarity solution, up to the third level of truncation, has been obtained for convective flow in the porous medium. The effects of solid boundary and inertia forces which have been neglected in the Darcy flow model were taken into account. Results were obtained for $Pr = 7$, 20, 50, and other parameters in the range of $0 \leqslant \Omega \leqslant 2.0$ and $0 \leqslant Ncc \leqslant 2.0$. For pure forced convection and low Ncc (nearly isothermal), the error resulting from omitting the boundary and inertia forces decreases with increasing downstream distance. For mixed convection flow the effects of boundary and inertia on local heat transfer coefficient and local heat flux become very significant at large values of Ncc, especially downstream.

INTRODUCTION

CONVECTIVE heat transfer in a porous medium has attracted considerable interest in recent years due to its numerous applications in industrial and geophysical problems. Excellent review articles are provided by Cheng [1, 2]. Most of the existing studies have been based on Darcy's law [3], which neglects the boundary and inertia effects on fluid flow and heat transfer.

The boundary effects are usually small for packed spheres since permeability is small. However, for certain solid materials, such as foametals fibrous media [4], where the permeability and porosity are high, the boundary effect cannot be neglected.

The inertia effects, though not important in low-porosity porous media, are shown to be very significant in high-porosity porous media [4]. The inertia effects also become important at high-speed flows in a porous medium.

In mechanical engineering, the subject probably becomes of greater importance with the use of porous materials of high porosity which have the form of a latticework of metallic or non-metallic fibers [4] where the boundary and inertia effects become more significant. The effects of boundary and inertia on heat transfer for constant high-porosity porous media were examined by Vafai and Tien [5] for forced convection, and by Ranganathan and Viskanta [6] for mixed convection. Results of their analyses have shown that both boundary and inertia effects decrease the velocity in the thermal boundary layer, broaden the temperature distribution, and reduce the heat transfer rates.

Most of the previous studies for heat transfer problems in porous media have been based on some assumed temperature distributions along the impermeable surface, and thus the solid–fluid interactions were neglected. Sparrow and Acharya [7], Sparrow and Chyu [8] and Sunden [9] concluded that, although the conventional fin theory model based on the prescribed uniform heat transfer coefficient gives a good estimate of the overall heat transfer rate from the fin, substantial errors could arise in the prediction of the local heat transfer rate. The conjugate mixed convection–conduction heat transfer problem for a plate fin embedded vertically in a saturated porous medium has recently been analyzed by Liu *et al.* [10], using Darcy's law, where both solid boundary and inertia forces were neglected.

The present investigation analyzes the effects of boundary and inertia forces on conjugate mixed convection–conduction heat transfer in a high-porosity porous medium. The local volume-averaging technique [5] is applied to the fundamental flow and energy equations in a porous medium. Both boundary and inertia effects are included in the equations. Since the developing region of the boundary layer for almost all practical cases is very small [5], the convective effects are neglected. The porous medium under study here is assumed to be made up of a latticework of metallic fibers, which is referred to as foametal [4]. The value of F (a function used to express inertia terms) which depends on permeability, geometry, and Reynolds number based on the square root of per-

† Present address: Marshall Space Flight Center, National Aeronautics and Space Administration, Huntsville, AL 35812, U.S.A.

NOMENCLATURE

Da	Darcy number, K/L^2
F	function used to express inertia term, defined in equation (1)
f	dimensionless stream function defined in equation (12a)
G	auxiliary dimensionless velocity function, $\partial f/\partial\xi$
Gr	Grashof number, $[g\beta_f K(T_b-T_\infty)L]/\nu_f^2$
$\mathbf{g}$	gravitational acceleration
H	auxiliary dimensionless velocity function, $\partial G/\partial\xi$
h	local heat transfer coefficient
h^*	dimensionless local heat transfer coefficient, $[h(x)L]/(k\sqrt{Re})$
$\bar{h}$	average heat transfer coefficient, defined in equation (60)
$\bar{h}^*$	dimensionless average heat transfer coefficient, $\bar{h}L/k\sqrt{Re}$
K	permeability of porous structure
k	equivalent thermal conductivity of the porous medium
k_s	fin thermal conductivity
L	fin length
Ncc	convection–conduction parameter, defined in equation (17)
Pe	Peclet number, $(u_\infty L)/\alpha$
Pr	Prandtl number, ν_f/α
Q	total heat transfer rate, defined in equation (64)
Q^*	dimensionless total heat transfer rate, $Q/[k(T_b-T_\infty)\sqrt{Re}]$
q	local heat flux
q^*	dimensionless local heat flux, $(qL)/[k(T_b-T_\infty)\sqrt{Re}]$
Re	Reynolds number, $(u_\infty L)/\nu_f$
T	temperature
T_b	fin base temperature
T_s	fin temperature
u	velocity in x-direction
v	velocity in y-direction
x	streamwise coordinate
y	transverse coordinate.

Greek symbols

α	effective thermal diffusivity
β_f	coefficient of thermal expansion of fluid
δ	plate fin half thickness
ε_f	porosity of the medium
η	pseudosimilarity variable, defined by equation (11b)
η_{eff}	fin efficiency, defined in equation (68)
θ	dimensionless temperature, $[T(x,y)-T_\infty]/(T_b-T_\infty)$
θ_s	dimensionless fin temperature, $[T_s(x)-T_\infty]/(T_b-T_\infty)$
Λ	inertia parameter, $Re\,F\varepsilon_f\sqrt{Da}$
μ_f	dynamic viscosity of fluid
ν_f	kinematic viscosity of fluid
ξ	transformed streamwise coordinate, defined by equation (11a)
ρ_f	density of fluid
ϕ	auxiliary dimensionless temperature function, $\partial\theta/\partial\xi$
χ	auxiliary dimensionless temperature function, $\partial\phi/\partial\xi$
ψ	stream function, defined by equation (12a)
Ω	buoyancy force parameter, Gr/Re.

Subscripts

b	condition at the fin base
f	quantities associated with the fluid
s	quantities associated with the fin
w	condition at the wall
∞	condition at infinity
η	differentiation with respect to η
ξ	differentiation with respect to ξ.

meability is taken as 0.07 [4]. Boundary layer approximations similar to those invoked by Wooding [11] and McNabb [12] are applicable. Numerical solutions have been obtained by the local non-similarity approximation [13, 14] and the results are compared with those of the Darcy flow model [10].

ANALYSIS

Consider a plate fin of length L and thickness 2δ, which is placed vertically downward in a saturated porous medium as shown in Fig. 1. The x and y denote, respectively, the streamwise and the transverse coordinates; and u and v are the velocities in the x- and y-directions. The temperature of the medium far away from the plate is T_∞, while the fin base temperature is maintained at a constant temperature T_b, and $T_b > T_\infty$. Under the assumptions that the porous medium is in local thermal equilibrium, the properties of the fluid and the porous matrix are constant, isotropic and homogeneous, and the boundary layer and Boussinesq approximation are also applicable, the governing equations for the flow field become

$$\frac{\mu_f}{\varepsilon_f}\frac{\partial^3\psi}{\partial y^3}-\frac{\rho_f F\varepsilon_f}{\sqrt{K}}\left(\frac{\partial\psi}{\partial y}\right)^2-\frac{\mu_f}{K}\frac{\partial\psi}{\partial y}+\frac{g\rho_f\beta_f}{\varepsilon_f}(T-T_\infty)+\frac{\mu_f u_\infty}{K}=0 \quad (1)$$

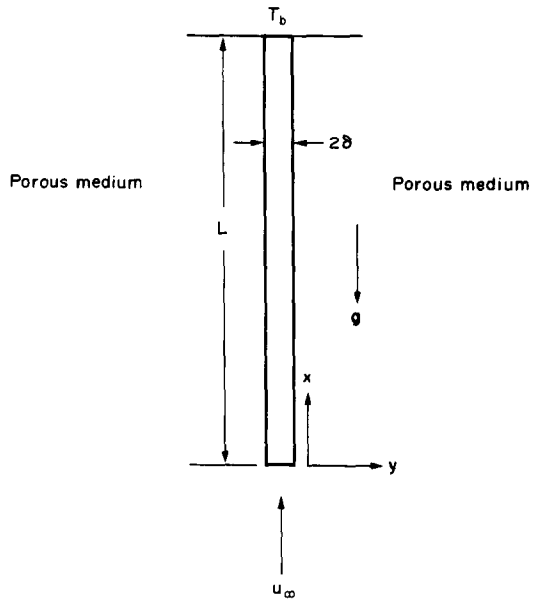

FIG. 1. Schematic diagram of the vertical plate fin.

$$\frac{\partial\psi}{\partial y}\frac{\partial T}{\partial x}-\frac{\partial\psi}{\partial x}\frac{\partial T}{\partial y}=\alpha\frac{\partial^2 T}{\partial y^2} \tag{2}$$

where the stream function ψ is defined as

$$u=\frac{\partial\psi}{\partial y};\quad v=-\frac{\partial\psi}{\partial x} \tag{3a,b}$$

F is a function used to express the inertia term; K is the permeability of the porous structure; and ε_f is the porosity of the medium.

The boundary conditions are

$$\frac{\partial\psi}{\partial y}=0;\quad \frac{\partial\psi}{\partial x}=0;\quad T=T_w(x)\ \text{at}\ y=0. \tag{4a–c}$$

The free stream velocity near the edge of the boundary layer can be obtained from equation (1) by neglecting the viscous and buoyancy terms and solving for $\partial\psi/\partial y$. Thus

$$\frac{\partial\psi}{\partial y}=u_\infty\left[\frac{-1+\sqrt{(1+4u_\infty F\varepsilon_f\sqrt{K/\nu_f})}}{2u_\infty F\varepsilon_f\sqrt{K/\nu_f}}\right];$$

$$T=T_\infty\ \text{at}\ y\to\infty. \tag{5a,b}$$

If the fin is considered to be relatively long compared with its thickness, a one-dimensional model for the fin temperature distribution can be assumed. In addition, the amount of heat which passes from the tip of the fin to the fluid is assumed to be negligible. Under these assumptions, the fin conservation equation and boundary conditions are

$$\frac{d^2T_s}{dx^2}=\frac{h(x)}{k_s\delta}(T_s-T_\infty) \tag{6}$$

$$\frac{dT_s}{dx}=0\quad\text{at}\ x=0 \tag{7}$$

$$T_s(x)=T_b\quad\text{at}\ x=L. \tag{8}$$

At the fluid–solid interface, $y=0$ (i.e. at the surface of the fin), it is required that the local temperature $T_w(x)$ and the local heat flux q be the same in the fluid and the solid. Thus

$$T(x,y)=T_s(x)\quad\text{at}\ y=0 \tag{9}$$

$$-k\frac{\partial T}{\partial y}(x,y)=h(x)[T_s(x)-T_\infty]\quad\text{at}\ y=0. \tag{10}$$

Equations (1) and (2) do not admit similarity solutions. The non-similarities arise from the temperature distribution of the fin and the buoyancy force. To solve this problem by the local non-similarity method, ξ and η coordinates are defined as

$$\xi=\frac{x}{L};\quad \eta=\sqrt{\left(\frac{u_\infty}{\alpha}\right)}\frac{y}{\sqrt{x}}. \tag{11a,b}$$

In addition, dimensionless stream function and temperature variables are introduced as follows:

$$\psi(x,y)=\sqrt{(\alpha u_\infty x)}f(\xi,\eta);$$

$$\theta(\xi,\eta)=\frac{T(x,y)-T_\infty}{T_b-T_\infty} \tag{12a,b}$$

where the dependence of f and θ with respect to ξ is weak.

Substitution of equations (11) and (12) into equations (1) and (2) leads to

$$\frac{Pe\,Da}{\varepsilon_f}\frac{\partial^3 f}{\partial\eta^3}-\Lambda\left(\frac{\partial f}{\partial\eta}\right)^2-\frac{\partial f}{\partial\eta}+\frac{\Omega\theta}{\varepsilon_f}+1=0 \tag{13}$$

$$\frac{\partial^2\theta}{\partial\eta^2}+\frac{f}{2}\frac{\partial\theta}{\partial\eta}=\xi\left(\frac{\partial f}{\partial\eta}\frac{\partial\theta}{\partial\xi}-\frac{\partial f}{\partial\xi}\frac{\partial\theta}{\partial\eta}\right) \tag{14}$$

where $Da=K/L^2$, $Pe=u_\infty L/\alpha$, $\Omega=Gr/Re$, $Gr=g\beta_f K(T_b-T_\infty)L/\nu_f^2$, $Re=u_\infty L/\nu_f$, and $\Lambda=Re\,F\varepsilon_f\sqrt{Da}$.

The boundary conditions are

$$\frac{\partial f}{\partial\eta}=0;\quad \xi\frac{\partial f}{\partial\xi}+\frac{f}{2}=0;\quad \theta=\theta_w\ \text{at}\ \eta=0 \tag{15a–c}$$

$$\frac{\partial f}{\partial\eta}=\frac{-1+\sqrt{(1+4\Lambda)}}{2\Lambda};\quad \theta=0\quad\text{at}\ \eta\to\infty. \tag{16a,b}$$

The transformed fin conservation equation and boundary conditions are

$$\frac{d^2\theta_s}{d\xi^2}=h^*(\xi)\,Ncc\,\theta_s(\xi) \tag{17}$$

$$\frac{d\theta_s}{d\xi}(\xi)=0\quad\text{at}\ \xi=0 \tag{18}$$

$$\theta_s(\xi)=1\quad\text{at}\ \xi=1 \tag{19}$$

where $h^*(\xi)=h(x)L/k\sqrt{Re}$ and $Ncc=(kL/k_s\delta)\sqrt{Re}$.

The transformed interfacial conditions are

$$\theta(\xi,\eta)=\theta_s(\xi)\quad\text{at}\ \eta=0 \tag{20}$$

$$-\frac{d\theta}{d\eta}(\xi,\eta)=\frac{h^*(\xi)\sqrt{\xi\theta_s(\xi)}}{\sqrt{Pr}} \quad \text{at } \eta=0 \tag{21}$$

where $Pr=\nu_f/\alpha$.

To obtain a solution to the problem, equations (13)–(16) must be solved simultaneously with equations (17)–(21).

Local non-similarity solution

The local non-similarity method [13] will now be applied to equations (13)–(16) to obtain a set of ordinary differential equations.

For the first level of truncation we neglect the terms involving $\partial f/\partial\xi$ and $\partial\theta/\partial\xi$ in equations (14) and (15b). With these approximations, equations (13)–(16) can be rewritten as

$$f_{\eta\eta\eta}+P_{1f}f_{\eta\eta}=Q_{1f} \tag{22}$$

$$\theta_{\eta\eta}+P_{1\theta}\theta_\eta=Q_{1\theta} \tag{23}$$

where

$$P_{1f}=0;\quad Q_{1f}=\frac{\varepsilon_f}{Pe\,Da}\frac{\xi}{}\left[(\Lambda f_\eta+1)f_\eta-\frac{\Omega\theta}{\varepsilon_f}-1\right] \tag{24a,b}$$

$$P_{1\theta}=\frac{f}{2};\quad Q_{1\theta}=0. \tag{25a,b}$$

Here, the first subscript on P and Q in equations (22) and (23) represents the truncation level while the second subscript denotes the dependent variable of the particular equation.

The boundary conditions are

$$f_\eta=0;\quad f=0;\quad \theta=\theta_s \quad \text{at } \eta=0 \tag{26a–c}$$

$$f_\eta=\frac{-1+\sqrt{(1+4\Lambda)}}{2\Lambda};\quad \theta=0 \quad \text{at } \eta\to\infty. \tag{27a,b}$$

For the second level of truncation, the governing equations for f and θ are retained without approximation by introducing $\partial f/\partial\xi=G$ and $\partial\theta/\partial\xi=\phi$. Equations (13)–(16) are differentiated with respect to ξ and after neglecting the terms involving $\partial G/\partial\xi$ and $\partial\theta/\partial\xi$ give auxiliary equations for G and ϕ with appropriate boundary conditions. Thus, for the second level of truncation

$$f_{\eta\eta\eta}+P_{2f}f_{\eta\eta}=Q_{2f} \tag{28}$$

$$\theta_{\eta\eta}+P_{2\theta}\theta_\eta=Q_{2\theta} \tag{29}$$

$$G_{\eta\eta\eta}+P_{2G}G_{\eta\eta}=Q_{2G} \tag{30}$$

$$\phi_{\eta\eta}+P_{2\phi}\phi_\eta=Q_{2\phi} \tag{31}$$

where

$$P_{2f}=0;\quad Q_{2f}=\frac{\varepsilon_f}{Pe\,Da}\frac{\xi}{}\left[(\Lambda f_\eta+1)f_\eta-\frac{\Omega\theta}{\varepsilon_f}-1\right] \tag{32a,b}$$

$$P_{2\theta}=\tfrac{1}{2}(f+2\xi G);\quad Q_{2\theta}=\xi f_\eta\phi \tag{33a,b}$$

$$P_{2G}=0;\quad Q_{2G}=\frac{\varepsilon_f}{Pe\,Da}\left[\xi(2\Lambda f_\eta+1)G_\eta+(\Lambda f_\eta+1)f_\eta-\frac{\xi\Omega\phi}{\varepsilon_f}-\frac{\Omega\theta}{\varepsilon_f}-1\right] \tag{34a,b}$$

$$P_{2\phi}=\tfrac{1}{2}(f+2\xi G);\quad Q_{2\phi}=[(f_\eta+\xi G_\eta)\phi-\tfrac{3}{2}G\theta_\eta] \tag{35a,b}$$

with boundary conditions

$$f_\eta=0;\quad \xi G+\frac{f}{2}=0;\quad \theta=\theta_s \quad \text{at } \eta=0 \tag{36a–c}$$

$$f_\eta=\frac{-1+\sqrt{(1+4\Lambda)}}{2\Lambda};\quad \theta=0 \quad \text{at } \eta\to\infty \tag{37a,b}$$

$$G_\eta=0;\quad G=0;\quad \phi=\frac{\partial\theta_s}{\partial\xi} \quad \text{at } \eta=0 \tag{38a–c}$$

$$G=0;\quad \phi=0 \quad \text{at } \eta\to\infty. \tag{39a,b}$$

For the third level of truncation, all terms involving $\partial G/\partial\xi$ and $\partial\phi/\partial\xi$ which have been neglected in the second level truncation are restored. Additional subsidiary equations and boundary conditions are obtained by differentiating all the second level equations (without approximations) with respect to ξ and neglecting terms involving $\partial H/\partial\xi$ and $\partial\chi/\partial\xi$. Thus the equations for the third level of truncation become

$$f_{\eta\eta\eta}+P_{3f}f_{\eta\eta}=Q_{3f} \tag{40}$$

$$\theta_{\eta\eta}+P_{3\theta}\theta_\eta=Q_{3\theta} \tag{41}$$

$$G_{\eta\eta\eta}+P_{3G}G_{\eta\eta}=Q_{3G} \tag{42}$$

$$\phi_{\eta\eta}+P_{3\phi}\phi_\eta=Q_{3\phi} \tag{43}$$

$$H_{\eta\eta\eta}+P_{3H}H_{\eta\eta}=Q_{3H} \tag{44}$$

$$\chi_{\eta\eta}+P_{3\chi}\chi_\eta=Q_{3\chi} \tag{45}$$

where

$$H=\frac{\partial G}{\partial\xi};\quad \chi=\frac{\partial\phi}{\partial\xi}$$

$$P_{3f}=0;\quad Q_{3f}=\frac{\varepsilon_f}{Pe\,Da}\frac{\xi}{}\left[(\Lambda f_\eta+1)f_\eta-\frac{\Omega\theta}{\varepsilon_f}-1\right] \tag{46a,b}$$

$$P_{3\theta}=\tfrac{1}{2}(f+2\xi G);\quad Q_{3f}=\xi f_\eta\theta \tag{47a,b}$$

$$P_{3G}=0;\quad Q_{3G}=\frac{\varepsilon_f}{Pe\,Da}\left[\xi(2\Lambda f_\eta+1)G_\eta+(\Lambda f_\eta+1)f_\eta-\frac{\xi\Omega\phi}{\varepsilon_f}-\frac{\Omega\theta}{\varepsilon_f}-1\right] \tag{48a,b}$$

$$P_{3\phi}=\tfrac{1}{2}(f+2\xi G);\quad Q_{3\phi}=[(f_\eta+\xi G_\eta)\phi-(\tfrac{3}{2}G+\xi H)\theta_\eta+\xi f_\eta\chi] \tag{49a,b}$$

$$P_{3H}=0;\quad Q_{3H}=\frac{\varepsilon_f}{Pe\,Da}\left\{\xi(2\Lambda f_\eta+1)H_\eta + [2\Lambda(\xi G_\eta+2f_\eta)+2]G_\eta-\frac{\Omega}{\varepsilon_f}(\xi\chi+2\phi)\right\} \quad (50a,b)$$

$$P_{3\chi}=\tfrac{1}{2}(f+2\xi G);\quad Q_{3\chi}=[2(f_\eta+\xi G_\eta)\chi - (3G+2\xi H)\phi_\eta+(2G_\eta+\xi H_\eta)\phi-\tfrac{5}{2}H\theta_\eta]. \quad (51a,b)$$

The boundary conditions are

$$f_\eta=0;\quad \xi G+\frac{f}{2}=0;\quad \theta=\theta_s \quad \text{at } \eta=0 \quad (52a\text{–}c)$$

$$f_\eta=\frac{-1+\sqrt{(1+4\Lambda)}}{2\Lambda};\quad \theta=0 \quad \text{at } \eta\to\infty. \quad (53a,b)$$

$$G_\eta=0;\quad \xi H+\tfrac{3}{2}G=0;\quad \phi=\frac{\partial\theta_s}{\partial\xi} \quad \text{at } \eta=0 \quad (54a\text{–}c)$$

$$G_\eta=0;\quad \phi=0 \quad \text{at } \eta\to\infty \quad (55a,b)$$

$$H_\eta=0;\quad H=0;\quad \chi=\frac{\partial^2\theta_s}{\partial\xi^2} \quad \text{at } \eta=0 \quad (56a\text{–}c)$$

$$H_\eta=0;\quad \chi=0 \quad \text{at } \eta\to\infty. \quad (57a,b)$$

RESULTS AND DISCUSSION

The heat conduction equation for the fin and the local non-similarity equations for the flow field can be converted into an integral form and numerical solutions can be obtained by iteration. The details of the procedure are described in ref. [10]. Computations were carried out up to the third level of truncation.

The numerical results presented in the figures are all for typical high, uniform-porosity ($\varepsilon_f = 0.98$) porous media and constant permeability ($K = 10^{-6}$ m^2). The typical Reynolds number, $Re = u_\infty L/\nu_f$ is taken as 49 700 for the following values of physical quantities: for water at $Pr = 7.0$, $\nu_f = 1.006\times10^{-6}$ m^2 s^{-1}, $L = 1.0$ m and $u_\infty = 0.05$ m s^{-1}. The buoyancy force parameter Ω and conjugate convection–conduction parameter Ncc are considered between the ranges of 0–0.2. To study the effects of Prandtl numbers, results are also obtained for $Pr = 20$ and 50.

Fin temperature distributions

The effects of boundary and inertia on fin temperature distributions are shown in Fig. 2 and compared with the results of the Darcy flow model [10]. The fin temperature variations decrease due to the boundary and inertia effects. The fin temperature distributions are also functions of Ncc and Ω. They all show the expected trend whereby the fin temperature distributions decrease monotonically from the fin base to the tip. Everything else remaining fixed, the effect of increasing Ncc implies a poorly conducting wall

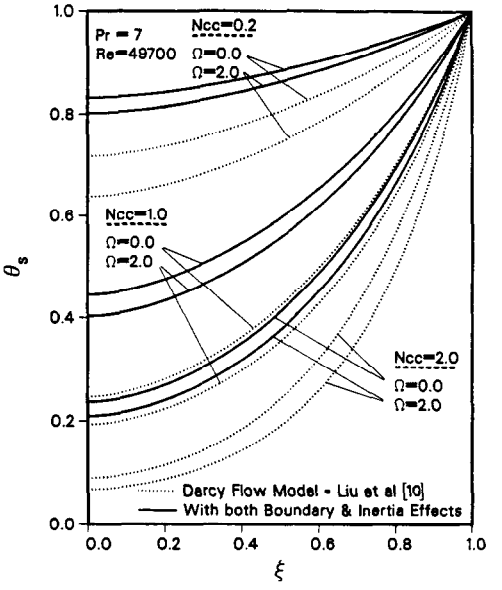

FIG. 2. Fin temperature distributions.

across which a greater temperature drop occurs. The larger values of Ω give rise to greater fin wall temperature variations. This is because the buoyancy force assists the flow and thus increases the convective heat transfer resulting in lower temperatures.

Local heat transfer coefficients

The local heat transfer coefficients can be determined at every position ξ from the expression

$$h(x)=\frac{-k\left[\dfrac{\partial T}{\partial y}(x,y)\right]_{y=0}}{T_s(x)-T_\infty} \quad (58)$$

or in dimensionless form

$$h^*(\xi)=\frac{h(x)L}{k\sqrt{Re}}=\frac{\sqrt{Pr}\,[-\theta_\eta(\xi,\eta)]_{\eta=0}}{\sqrt{\xi}\quad\theta_s(\xi)}. \quad (59)$$

The distributions of local heat transfer coefficients with conjugate effect are presented in Fig. 3. It can be seen that the boundary and inertia forces reduce the local heat transfer coefficients. For $\Omega = 0$ (pure forced convection) at low Ncc (nearly isothermal), the error resulting from omitting the boundary and inertia force decreases with increasing downstream distance. However, for mixed convection flow at large Ncc, the error is much higher, especially downstream.

The present analysis also reveals that for forced convection, the heat transfer coefficient tends to decrease monotonically from an infinite value at the tip to some value at the fin base for all values of Ncc. For mixed convection flows at low Ncc ($Ncc = 0.2$), the distributions of local heat transfer coefficients closely approximate those for an isothermal fin, where they decrease monotonically from the tip to the base, with the variations being relatively rapid near the

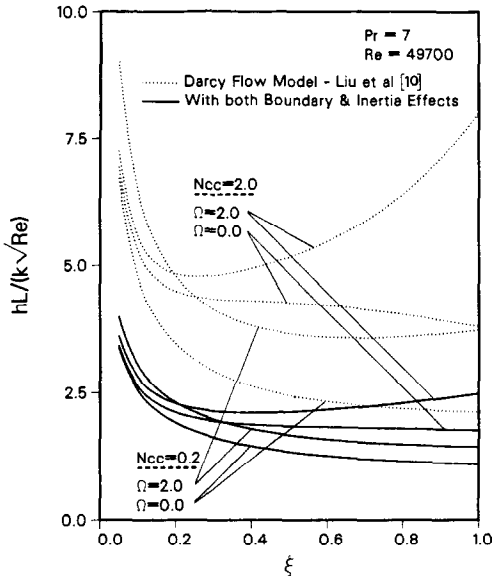

FIG. 3. Local heat transfer coefficients.

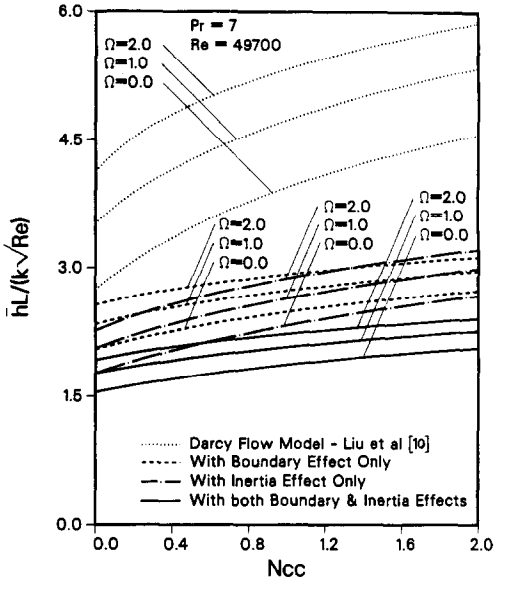

FIG. 4. Average heat transfer coefficients.

tip and more gradual near the base. At higher *Ncc*, there is an initial drop in the heat transfer coefficient which becomes more and more gradual with increasing ξ, and ultimately leads to a minimum after which it increases steadily with ξ. At higher *Ncc*, the location of the minimum also shifts towards the tip, and the extent of the downstream rise becomes greater.

Average heat transfer coefficients

The average heat transfer coefficient can be obtained by integrating the local heat transfer coefficient over the fin surface and dividing by the fin length. It can be expressed in both dimensional and non-dimensional forms as

$$\bar{h} = \frac{1}{L}\int_0^L h(x)\,\mathrm{d}x \tag{60}$$

$$\bar{h}^* = \frac{\bar{h}L}{k\sqrt{Re}}. \tag{61}$$

Figure 4 shows the effects of boundary and inertia on the average heat transfer coefficients as a function of *Ncc*. The boundary effect decreases the average heat transfer coefficient and becomes more pronounced at higher *Ncc*. The inertia effect also decreases the average heat transfer coefficient. The average heat transfer coefficient also increases as Ω increases and *Ncc* increases. This is due to the fact that larger values of the local heat transfer coefficient prevail in most of the fin length for larger *Ncc*.

Figure 5 shows the effects of Prandtl numbers on average heat transfer coefficients as a function of buoyancy force. The average heat transfer coefficients are higher for high Prandtl number fluids. As *Ncc* is increased, the influence of *Pr* becomes more pronounced.

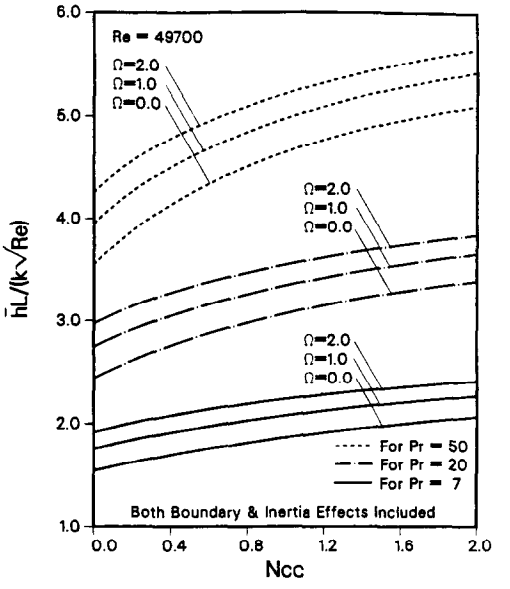

FIG. 5. Effects of Prandtl numbers of average heat transfer coefficients.

Local heat fluxes

The local heat flux can be computed from

$$q(x) = -k\left[\frac{\partial T}{\partial y}(x,y)\right]_{y=0} \tag{62}$$

and in dimensionless form from

$$q^*(\xi) = \frac{q(x)L}{k(T_b - T_\infty)\sqrt{Re}} = \frac{\sqrt{Pr}}{\sqrt{\xi}}[-\theta_\eta(\xi,\eta)]_{\eta=0}. \tag{63}$$

The influence of boundary and inertia forces on local heat flux variations at the solid–fluid interface is

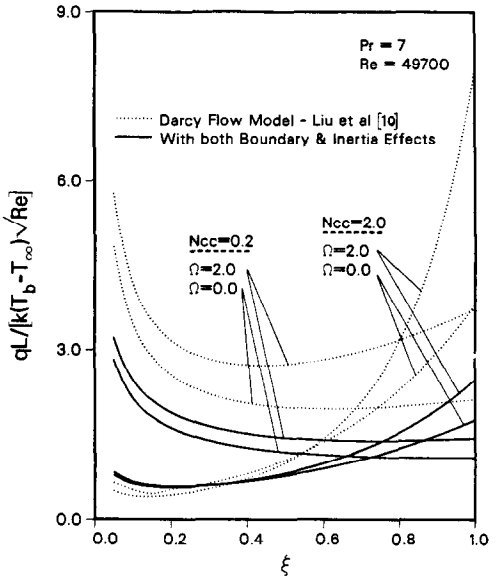

FIG. 6. Local heat fluxes

plotted in Fig. 6 as a function of Ω. The figure shows that the boundary and inertia effects reduce the heat transfer and these effects become more significant at higher buoyancy forces and *Ncc*, especially downstream. In the figure, for mixed convection flows, it can be seen that as Ω increases, local heat flux increases over the major part of the surface. Small values of *Ncc* yield high values of heat flux near the tip and lower values near the root. This finding stands in contrast to the conventional perception that the highest rates of convective heat transfer always occur adjacent to the root. As *Ncc* increases, the heat flux first decreases, reaches a minimum and then starts to increase. At high *Ncc*, most of the heat transfer takes place near the fin base. This is due to the strong buoyancy force near the fin base. However, in the vicinity of the leading edge, the influence of the buoyancy force is very small. For high *Ncc*, the temperature close to the leading edge is small, and thus, the buoyancy force has little effect.

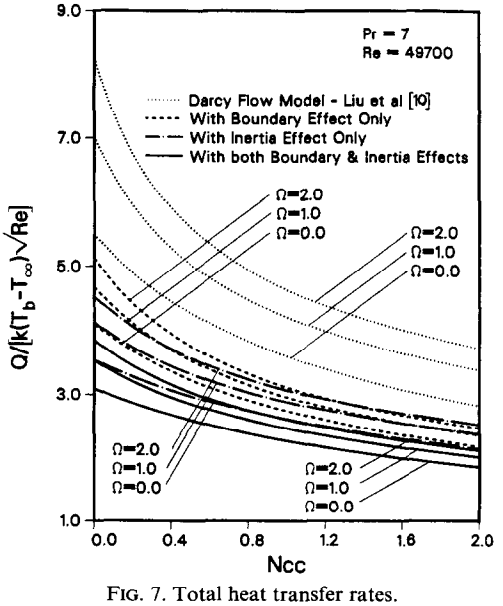

FIG. 7. Total heat transfer rates.

Total heat transfer rates

The total heat transfer rate can be obtained from the solutions either by integrating the local heat flux at the fin surface or from the heat conducted from the base surface at $\xi = 1$ to the fin. Thus

$$Q = 2\int_0^L q(x)\,dx \tag{64}$$

or

$$Q = 2k_s\delta\left[\frac{\Delta T_s}{\partial x}(x)\right]_{x=L}. \tag{65}$$

In dimensionless forms, these become

$$Q^* = \frac{Q}{k(T_b - T_\infty)\sqrt{Re}} = 2\sqrt{Pr}\int_0^1 \left\{\frac{[-\theta_\eta(\xi,\eta)]_{\eta=0}}{\sqrt{\xi}}\right\}d\xi \tag{66}$$

or

$$Q^* = \frac{Q}{k(T_b - T_\infty)\sqrt{Re}} = \frac{2}{Ncc}\left[\frac{d\theta_s}{d\xi}(\xi)\right]_{\xi=1}. \tag{67}$$

Total heat transfer rates solved by the two methods are found to be in good agreement. In Fig. 7, it is shown that the total heat transfer rates decrease due to the inertia effect. The inertia effect becomes more important at higher Ω. The boundary effect also results in a smaller total heat transfer rate. Both boundary and inertia effects on total heat transfer rates are more significant at lower *Ncc*. The total heat transfer rate increases as buoyancy force increases.

Figure 8 shows the combined influence of the Prandtl number and *Ncc* on total heat transfer rates. The figure shows that for fixed values of *Ncc* and Ω, the higher *Pr* result in large heat transfer rates.

Fin efficiencies

The fin efficiency is defined as the ratio of the total heat transfer rate of the fin to the heat transfer rate of an isothermal fin, or

$$\eta_{eff} = \frac{Q^*}{[Q^*]_{Ncc=0}}. \tag{68}$$

The combined influence of buoyancy force and the convection–conduction parameter on fin efficiency is provided in Fig. 9. With increasing values of *Ncc* and Ω, the fin efficiency is decreased. This result is similar to that in ref. [9] for a classical fluid. It should also be noted that the heat transfer from the corresponding isothermal fin is not the same for flows with and without boundary and inertia forces. Thus the smaller

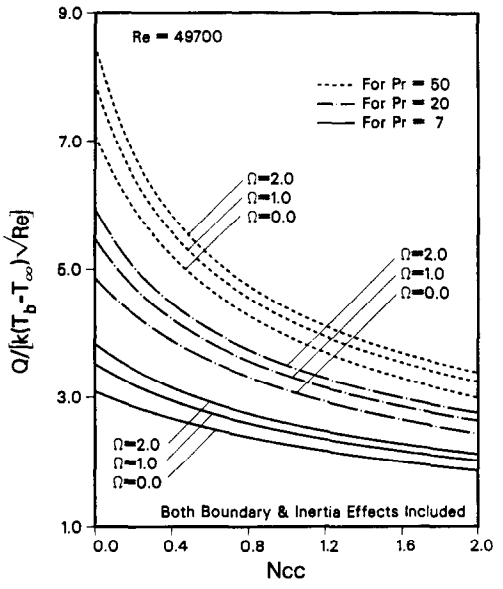

FIG. 8. Effects of Prandtl numbers on total heat transfer rates.

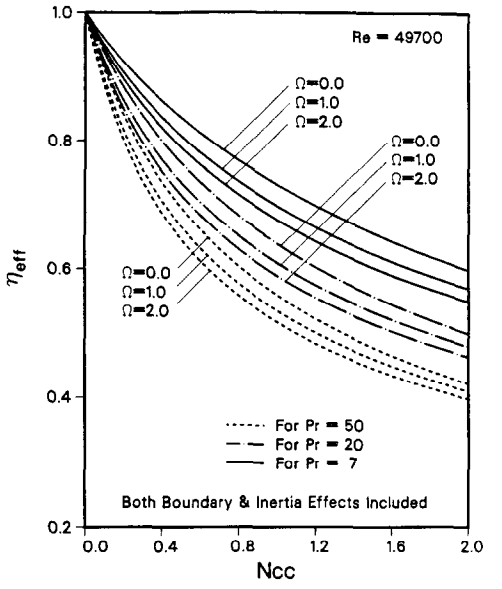

FIG. 10. Effects of Prandtl numbers on fin efficiencies.

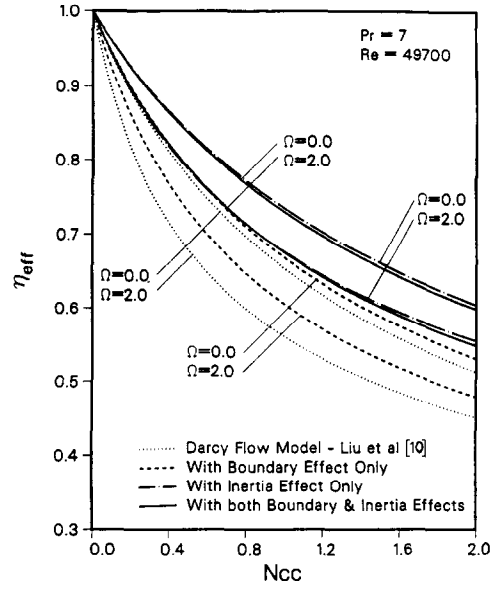

FIG. 9. Fin efficiencies.

values of η_{eff} does not mean that the heat transfer rate is also small.

In Fig. 10, the combined effect of the Prandtl number and the convection–conduction parameter on the fin efficiency is provided. With increasing values of *Ncc* and *Pr*, the fin efficiency is decreased. The influence of *Pr* on fin efficiency becomes larger as *Ncc* is increased.

CONCLUSION

The purpose of this analysis is to improve the Darcy flow model by including boundary and inertia effects in the governing equations. When these effects are included, the heat transfer coefficients and heat transfer rates are further decreased. Although the boundary layer thickness is usually small, neglecting the boundary effect might lead to a considerable error in the computation of heat transfer rate. For forced convection and low *Ncc*, the error in the heat transfer coefficient from omitting these effects decreases with increasing downstream distance. For mixed convection at higher *Ncc*, the error becomes much larger especially downstream. The boundary and inertia forces have significant effects on local heat flux for higher Ω and *Ncc*.

REFERENCES

1. P. Cheng, Heat transfer in geothermal systems, *Adv. Heat Transfer* **14,** 1–105 (1978).
2. P. Cheng, Natural convection in porous medium: external flows, NATO Advanced Study Institute on Natural Convection: Fundamentals and Applications, Izmir, Turkey, 16–27 July (1984).
3. H. Darcy, *Les Fontaines Publiques de la Ville de Dijon.* Dalmon, Paris (1856).
4. G. S. Beavers and E. M. Sparrow, Non-Darcy flow through fibrous porous media, *J. Appl. Mech.* **36,** 711–714 (1969).
5. K. Vafai and C. L. Tien, Boundary and inertia effects on flow and heat transfer in porous media, *Int. J. Heat Mass Transfer* **24,** 195–203 (1981).
6. R. Ranganathan and R. Viskanta, Mixed convection boundary layer flow along a vertical porous medium, *Numer. Heat Transfer* **7,** 305–317 (1984).
7. E. M. Sparrow and S. Acharya, A natural convection fin with a solution-determined nonmonotonically varying heat transfer coefficient, *J. Heat Transfer* **103,** 218–225 (1981).
8. E. M. Sparrow and M. K. Chyu, Conjugate forced convection–conduction analysis of heat transfer in a plate fin, *J. Heat Transfer* **104,** 204–206 (1982).
9. B. Sunden, Conjugate mixed convection heat transfer

from a vertical rectangular fin, *Int. Commun. Heat Mass Transfer* **10,** 267–276 (1983).
10. J. Y. Liu, W. J. Minkowycz and P. Cheng, Conjugate mixed convection heat transfer analysis of a plate fin embedded in a porous medium, *Numer. Heat Transfer* **9,** 575–590 (1986).
11. R. A. Wooding, Convection in a saturated porous medium of large Rayleigh number or Peclet number, *J. Fluid Mech.* **15,** 527–544 (1963).
12. A. McNabb, On convection in porous medium, *Proceedings of the Second Australian Conference on Hydraulic and Fluid Mechanics*, University of Aukland, Aukland, New Zealand, pp. c161–c171 (1965).
13. W. J. Minkowycz and E. M. Sparrow, Numerical solution scheme for local nonsimilarity boundary-layer analysis, *Numer. Heat Transfer* **1,** 69–85 (1978).
14. W. J. Minkowycz and E. M. Sparrow, Interaction between surface mass transfer and transverse curvature in natural convection boundary layers, *Int. J. Heat Mass Transfer* **22,** 1445–1454 (1979).

EFFETS DE LIMITE ET D'INERTIE SUR LA CONVECTION THERMIQUE MIXTE CONJUGUEE POUR UNE AILETTE PLANE VERTICALE DANS UN MILIEU A FORTE POROSITE

Résumé—On étudie la convection thermique mixte, conjuguée le long d'une ailette plane verticale noyée dans un milieu poreux à forte porosité. Une solution locale non-similaire, jusqu'au troisième niveau de troncature, est obtenue pour l'écoulement convectif dans un milieu poreux. Les effets de frontière solide et de force d'inertie qui sont négligés dans le modèle d'écoulement de Darcy sont pris en compte. Des résultats sont obtenus pour $Pr = 7, 20, 50$; $0.0 \leqslant \Omega \leqslant 2.0$ et $0.0 \leqslant Ncc \leqslant 2.0$. Pour la convection forcée pure et un faible Ncc (proche de l'isothermicité), l'erreur résultant de l'omission de limite et d'inertie diminue quand la distance en aval augmente. Pour l'écoulement de convection mixte, les effets de limite et d'inertie sur le coefficient de transfert thermique et le flux thermique locaux devient important aux grandes valeurs de Ncc, particulièrement en aval.

RAND- UND TRÄGHEITSEFFEKTE BEI MISCHKONVEKTION AN EINER VERTIKALEN RIPPE IN EINEM HOCHPORÖSEN STOFF

Zusammenfassung—Der Wärmeübergang bei Mischkonvektion an einer vertikalen Rippe in einem gesättigten hochporösen Medium wurde untersucht. Es wurde eine örtliche Nicht-Ähnlichkeitslösung bis zur dritten Ordnung für die Konvektionsströmung im porösen Medium ermittelt. Die Einflüsse der festen Berandung und die Trägheitseffekte, die beim Strömungsmodell von Darcy vernachlässigt wurden, sind hier berücksichtigt. Es liegen Ergebnisse für $Pr = 7; 20; 50$ im Bereich $0,0 \leqslant \Omega \leqslant 2,0$ und $0,0 \leqslant Ncc \leqslant 2,0$ vor. Bei reiner erzwungener Konvektion und kleinem Ncc (d. h. fast isothermen Bedingungen) verringert sich stromabwärts der Fehler, der sich durch die Vernachlässigung der Rand- und Trägheitskräfte ergibt. Bei Mischkonvektion werden die Einflüsse des Randes und der Trägheit auf den lokalen Wärmeübergangskoeffizienten und die lokale Wärmestromdichte bei großen Werten von Ncc, besonders stromabwärts, sehr bedeutsam.

ВЛИЯНИЕ ГРАНИЦ И ИНЕРЦИОННЫХ СИЛ НА СОПРЯЖЕННЫЙ ТЕПЛОПЕРЕНОС ОТ ВЕРТИКАЛЬНОГО ПЛОСКОГО РЕБРА В ВЫСОКОПОРИСТОЙ СРЕДЕ ПРИ СМЕШАННОЙ КОНВЕКЦИИ

Аннотация—Изучен сопряженный теплоперенос вдоль вертикального плоского ребра, погруженного в насыщенную высокопористую среду, при смешанной конвекции. Для конвективного течения в пористой среде получено локальное неавтомодельное решение с точностью до членов третьего порядка малости. Учитываловь влияние твердой границы и инерционных сил, которыми пренебрегают в модели Дарси. Получены результаты для $Pr = 7, 20, 50$ и для других параметров в диапазоне $0,0 \leqslant \Omega \leqslant 2,0$ и $0,0 \leqslant Ncc \leqslant 2,0$. Для чисто вынужденной конвекции и низких Ncc (почти изотермическое течение) ошибка, вызванная неучетом границ и инерционных сил, уменьшается с увеличением расстояния вниз по потоку. Для смешанной конвекции влияние границ и инерционных сил на локальный теплоперенос становится существенным при больших значениях Ncc, особенно вниз по потоку.